Nematic State in $CeAuSb_2$

S. Seo,[1,*] Xiaoyu Wang,[2] S. M. Thomas,[1] M. C. Rahn,[1,†] D. Carmo,[3] F. Ronning,[1] E. D. Bauer,[1] R. D. dos Reis,[3] M. Janoschek,[1,4] J. D. Thompson,[1] R. M. Fernandes,[5] and P. F. S. Rosa[1]

[1]*Los Alamos National Laboratory, Los Alamos, New Mexico 87545, USA*
[2]*James Frank Institute, University of Chicago, Chicago, Illinois 60615, USA*
[3]*Brazilian Synchrotron Light Laboratory (LNLS), Campinas, Sao Paulo 13083-100, Brazil*
[4]*Laboratory for Scientific Developments and Novel Materials, Paul Scherrer Institut, 5232 Villigen PSI, Switzerland*
[5]*School of Physics and Astronomy, University of Minnesota, Minneapolis, Minnesota 55455, USA*

(Received 7 August 2019; revised manuscript received 5 November 2019; accepted 25 December 2019; published 13 February 2020; corrected 28 July 2020)

At ambient pressure and zero field, tetragonal $CeAuSb_2$ hosts stripe antiferromagnetic order at $T_N = 6.3$ K. Here, we first show via bulk thermodynamic probes and x-ray diffraction measurements that this magnetic order is connected with a structural phase transition to a superstructure that likely breaks C_4 symmetry, thus signaling nematic order. The temperature-field-pressure phase diagram of $CeAuSb_2$ subsequently reveals the emergence of additional ordered states under applied pressure at a multicritical point. Our phenomenological model supports the presence of a vestigial nematic phase in $CeAuSb_2$ akin to iron-based high-temperature superconductors; however, superconductivity, if present, remains to be discovered.

DOI: 10.1103/PhysRevX.10.011035

Subject Areas: Condensed Matter Physics, Strongly Correlated Materials

I. INTRODUCTION

Heavy-fermion systems, which consist of a lattice of f electrons that hybridize with the conduction electron sea, host prototypical examples of strongly correlated electronic states [1–4]. In particular, tetragonal Ce-based compounds often reveal novel quantum states of matter in the vicinity of a quantum critical point (QCP) at which a magnetic transition is suppressed to zero temperature by nonthermal parameters, e.g., pressure, magnetic field, or chemical doping [5,6]. Non-Fermi liquid (NFL) behavior, complex magnetic order, charge order, and unconventional superconductivity (SC) are examples of these states, which have also been observed in copper-oxide and iron pnictide high-T_c superconductors, although often accompanied by electronic nematicity—an electronic state that breaks the rotational symmetry of the underlying lattice but not its translational symmetry [7–9]. The origin of the nematic state, as well as its role on the superconducting state, remains controversial [10]. More recently, evidence for nematicity at high magnetic fields has been found in the heavy-fermion $CeRhIn_5$ [11], indicating that superconductivity and nematicity may also be intertwined in this class of strongly correlated materials [12]. Recent magnetostriction and nuclear magnetic resonance experiments point to the importance of crystalline electric field (CEF) effects in the putative nematic state of $CeRhIn_5$ [13,14].

$CeTSb_2$ (T = transition metal) is also a dense Kondo lattice system with pronounced CEF effects [15,16]. The magnetic and CEF ground states of $CeTSb_2$ depend on the transition metal T [16,17], and $CeAuSb_2$ orders antiferromagnetically below $T_N = 5$–6.8 K depending on the occupancy of the Au site [18–20]. Previous x-ray and neutron diffraction measurements showed that $CeAuSb_2$ crystallizes in a tetragonal crystal structure ($P4/nmm$) [21,22]. Pressurizing $CeAuSb_2$ does not suppress T_N to zero temperature but rather induces new phases hindering the appearance of a QCP or SC [20]. The nature of the pressure-induced phases in $CeAuSb_2$ remains an open question but possibly stems from competing magnetic interactions known to exist in this series of compounds [23,24]. In view of field-dependent properties of $CeAuSb_2$ at atmospheric pressure [19], application of magnetic fields could shed light on the evolution of the magnetic interactions in $CeAuSb_2$ under pressure. Unlike pressure, however, magnetic fields are symmetry breaking and tend to localize $4f$ electrons. In $CeAuSb_2$, T_N is gradually

*Corresponding author.
soonbeom@lanl.gov
†Present address: Institute for Solid State and Materials Physics, Technical University of Dresden, 01062 Dresden, Germany.

Published by the American Physical Society under the terms of the Creative Commons Attribution 4.0 International license. Further distribution of this work must maintain attribution to the author(s) and the published article's title, journal citation, and DOI.

suppressed by magnetic fields applied along the c axis, and two metamagnetic (MM) transitions are observed at $H_{c1} \sim 2.8$ T and $H_{c2} \sim 5.6$ T at low temperatures [18]. The H-T phase diagram constructed by magnetoresistance measurements reveals that both MM transitions are first order at low temperature [19]. In addition, H_{c2} has a tricritical point at 3.7 K, which may be suppressed under applied pressure [19]. A recent neutron diffraction study revealed that at H_{c1} the magnetic structure changes from a single-q striped phase with wave vector $\mathbf{Q}_1 = (\eta, \eta, 1/2)$ $[\eta = 0.136(2)]$ to a multi-q (woven or checkered) phase with $\mathbf{Q}_1 = (\eta, \eta, 1/2)$ and $\mathbf{Q}_2 = (\eta, -\eta, 1/2)$ [22]. This ground-state competition again stems from competing magnetic interactions and resembles the single-q to double-q magnetic transition observed in pnictides [25]. Furthermore, striped phases appear to be ubiquitous in strongly correlated systems including manganites, cuprates, nickelates, and cobaltites [26–29].

Remarkably, both striped and woven magnetic phases in $CeAuSb_2$ have twofold rotational symmetry in the ab plane even though the underlying lattice has fourfold rotational symmetry at high temperatures. As a result, one expects that the lattice will also break tetragonal C_4 symmetry in the presence of magnetoelastic coupling. In fact, in-plane uniaxial pressure experiments show that the magnetic transitions of $CeAuSb_2$ are sensitive to strain [30,31]. The situation thus seems analogous to iron-based high-T_c superconductors such as NaFeAs ("111") and LaFeAsO ("1111"), which share the same $P4/nmm$ space group as $CeAuSb_2$ [32,33]. There, the stripe magnetic order is generally preceded by a nematic phase with broken C_4 symmetry of the underlying lattice, in agreement with general theoretical expectations [34–37].

Here, we investigate whether such a nematic state exists in heavy-fermion $CeAuSb_2$. Bulk thermodynamic probes show the presence of two transitions at about 6.5 K and 6.3 K in $CeAuSb_2$ at ambient pressure. X-ray diffraction measurements reveal that the development of zero-field striped magnetic order is connected to a structural transition. Our phenomenological model proposes that this structural transition must be a nematic transition at $T_{\mathrm{nem}} \geq T_N$. Our results support the scenario in which $CeAuSb_2$ hosts a nematic phase that is not intertwined with superconductivity.

II. METHODS

Single crystals of $CeAuSb_2$ were synthesized by a self-flux method described in Ref. [19]. The highest T_N of 6.8 K is achieved in the electrical resistivity when the crystals are close to being stoichiometric, i.e., an average site occupancy of 100% of Au and residual resistivity ratio (RRR) of about 20. Samples with Au deficiency tend to have lower T_N [18,38]. Single crystals were pressurized to 2.66 GPa using a hybrid Be-Cu/NiCrAl clamp-type pressure cell. Daphne oil 7373 was used as a pressure-transmitting medium, and lead was used as a manometer [39]. The in-plane electrical resistivity of $CeAuSb_2$ was measured using a conventional four-probe technique with an LR700 Resistance Bridge in ^{4}He and ^{3}He cryostats from 300 K to 0.3 K. Magnetization measurements were performed using a commercial superconducting quantum interference device (SQUID), and the specific heat was measured using a commercial small-mass calorimeter that employs a quasi-adiabatic thermal relaxation technique. Thermal expansion along the c axis was measured at atmospheric pressure using a capacitance cell dilatometer with a resolution in $\Delta L/L$ of 10^{-8}. X-ray powder diffraction (XPD) measurements were performed at the x-ray diffraction and spectroscopy (XDS) beamline of the Brazilian Synchrotron Light Laboratory in Campinas, which uses a 4-T superconducting multipolar wiggler source [40]. The XPD patterns were collected at 20 keV in a transmission geometry using an area detector (MAR345). The sample was mounted at the cold finger of an open-cycle He cryostat (base temperature 2.3 K).

III. RESULTS

Specific heat, magnetic susceptibility, and thermal expansion measurements in $CeAuSb_2$ reveal two closely lying transitions. As shown in Fig. 1(a), and highlighted in the inset of Fig. 1(b), two peaks occur in the specific heat at $T_{\mathrm{nem}} = 6.48$ K and $T_N = 6.33$ K, indicated by arrows. Figure 1(c) shows the temperature dependence of the magnetic susceptibility for $H||[001]$, and the presence of two distinct phase transitions is evident in the derivative $\mathrm{d}\chi/dT$ at $T_{\mathrm{nem}} = 6.53$ K and $T_N = 6.33$ K shown in the inset. We note that the signatures of the two phase transitions in $CeAuSb_2$ in both specific heat and $\mathrm{d}\chi/dT$ are similar to those found in $BaFe_2As_2$ due to the nematic and magnetic transitions [41,42]. Figure 1(d) shows the temperature dependence of the c-axis length change, $\Delta L_c/L_c$, with an anomaly in the vicinity of 6.5 K. This anomaly is not typical of purely magnetic phase transitions [43,44], and the linear thermal-expansion coefficient, $\alpha_c = (1/L_c)(dL_c/dT)$, further reveals a negative peak at $T_{\mathrm{nem}} = 6.55$ K as well as a positive peak at $T_N = 6.33$ K, respectively [see inset of Fig. 1(d)]. Here, T_{nem} and T_N decrease together when fields are applied along the c axis, suggesting a strong coupling of the order parameters associated with these transitions. As shown below, T_{nem} is associated with a structural transition that likely breaks C_4 symmetry and T_N with a magnetic transition to the single-q stripe phase.

X-ray powder diffraction patterns of $CeAuSb_2$ measured at $T = 7$ K and $T = 3$ K are shown in Fig. 2. Rietveld refinement of the 7-K data in the published structure [46] provides a satisfactory fit in the $P4/nmm$ cell with lattice parameters $a = 4.3954(2)$ Å and $c = 10.318(1)$ Å. As indicated by the black difference line $[I(3\mathrm{K}) - I(7\mathrm{K})]$ in Fig. 2, the intensities of most Bragg peaks change

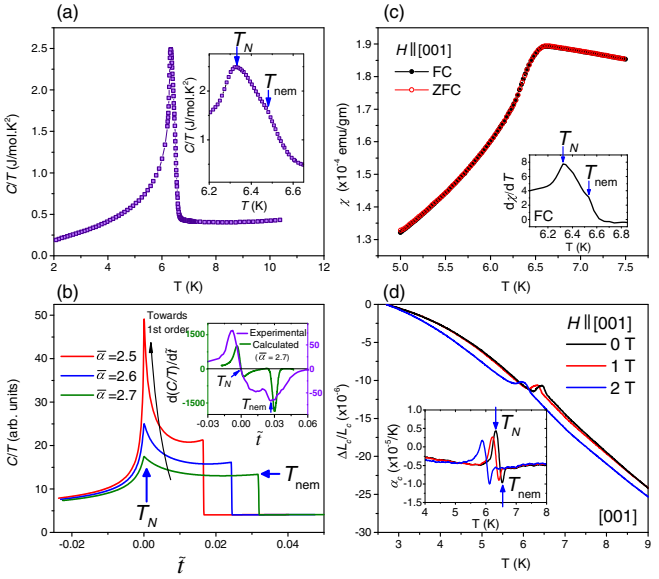

FIG. 1. (a) Specific heat divided by temperature of $CeAuSb_2$ at ambient pressure. The inset is a magnified view near the peak position. Arrows indicate the transition temperatures $T_{\rm nem}$ and T_N. (b) Calculated C/T versus reduced temperature for fixed anisotropy ζ and various inverse nematic coupling strength $\bar{\alpha}$. The inset gives the derivative of C/T of the experimental data (purple) and of the calculations with $\bar{\alpha} = 2.7$ (green). The theoretical curve was shifted and averaged over disorder for better comparison with the experimental data; details are given in the Supplemental Material [45]. (c) Temperature-dependent magnetic susceptibility in an applied field of 1 kOe along the c axis. ZFC (zero-field cooled; open circles) and FC (field-cooled; solid circles) curves show two transitions without hysteresis. The inset plots the derivative $\mathrm{d}\chi/\mathrm{d}T$. (d) Temperature dependence of the thermal expansion $\Delta L/L$ of $CeAuSb_2$ along [001] at zero field, 1 T, and 2 T applied along the c axis. The inset gives the thermal expansion coefficient.

(i.e., increase or decrease) below $T_N/T_{\rm nem}$, whereas a number of intensities also appear unaffected. Within the limited resolution of this experiment ($\Delta d/d > 10^{-4}$), we observe no evidence for a lattice distortion. As illustrated by the insets in Fig. 2, however, four peaks appear at low temperatures, which are not indexed in the parent phase and thus confirm that the true symmetry of the low-temperature phase of $CeAuSb_2$ is lower than that of the $P4/nmm$ space group. Because of the powder average and the limited number of observed intensities in the present data set, the full solution of the low-temperature modulated structure will have to await a single crystal diffraction study. Nevertheless, the absence of nuclear satellite peaks in neutron diffraction measurements [22] suggests that the x-ray diffraction superstructure peaks are due to a modulation of charge density, which is intimately coupled to the magnetic order parameter.

The existence of a magnetic ordered state that breaks a point-group symmetry (i.e., tetragonal symmetry), besides time-reversal and translational symmetry, suggests that the phase transition can happen in two stages [37]: At $T_{\rm nem}$, tetragonal symmetry is broken, whereas at T_N, both time-reversal and translational symmetries are broken. While it is challenging to develop a microscopic model for $CeAuSb_2$ that can account for the magnetic and nematic phase transitions in this compound, the thermodynamic properties such as specific heat can be obtained from an appropriate phenomenological model. We consider such a model by using a uniform stripe magnetic order with a two-component order parameter $\mathbf{m} = (\mathbf{m_1}, \mathbf{m_2})$, with ordering wave vectors $\mathbf{Q}_1 = (\eta, \eta, 1/2)$ and $\mathbf{Q}_2 = (\eta, -\eta, 1/2)$ for $\mathbf{m_1}$ and $\mathbf{m_2}$, respectively. Note that these two ordering vectors are not equivalent in the $P4/nmm$ group, but they are related by a 90° rotation. Up to quartic terms, the Ginzburg-Landau free energy compatible with the symmetries present in $CeAuSb_2$ is given by

$$F = \frac{1}{2} r_0 (\mathbf{m}_1^2 + \mathbf{m}_2^2) + \frac{u}{4} (\mathbf{m}_1^2 + \mathbf{m}_2^2)^2 - \frac{g}{4} (\mathbf{m}_1^2 - \mathbf{m}_2^2)^2, \tag{1}$$

where $r_0 \propto T - T_N^0$, $u > 0$. This result is identical to the free energy employed to understand the nematic phase of the pnictides [36]. Here, for simplicity, we consider both $\mathbf{m_1}$ and $\mathbf{m_2}$ to be real and that contributions from higher harmonics are neglected. Within a mean-field approximation, at $T < T_N^0$, the free energy is minimized for $0 < g < u$ by developing a stripe magnetic order, with either $\langle \mathbf{m_1} \rangle$ or $\langle \mathbf{m_2} \rangle$ becoming nonzero. Such a magnetic order also breaks C_4 symmetry down to C_2. Therefore, T_N^0 marks a simultaneous second-order nematic and magnetic phase transition.

So far, this analysis has neglected the gradient terms in Eq. (1), which describe contributions of magnetic fluctuations to the free energy. Going beyond mean-field analysis and including the effects of magnetic fluctuations, this model generally predicts a nematic transition at $T_{\rm nem} \geq T_N$, where T_N is the renormalized magnetic transition temperature to the stripe phase [36]. Such a paramagnetic-nematic state is characterized by anisotropic magnetic fluctuations, $\langle \mathbf{m_1}^2 - \mathbf{m_2}^2 \rangle \neq 0$, which spontaneously break the C_4 symmetry of the system even though $\langle \mathbf{m_1} \rangle = \langle \mathbf{m_2} \rangle = 0$. The fate of the coupled magnetic-nematic transitions depends on the parameters of the phenomenological model, which in our case are the degree of anisotropy of the magnetic fluctuations and the nematic coupling strength. The former is given by the ratio $\zeta \equiv J_z/J$ between the out-of-plane and in-plane effective exchange interactions, whereas the latter is given by the ratio $\bar{\alpha} \equiv u/g$ of the coefficients of Eq. (1). As shown previously in Ref. [36], for a fixed ζ, large $\bar{\alpha}$ gives two second-order transitions at $T_{\rm nem} > T_N$, whereas small $\bar{\alpha}$ gives a simultaneous first-order transition. In the intermediate $\bar{\alpha}$ range, two transitions remain, but one of them becomes first order [36] (see Supplemental Material [45] for details). We computed the entropy and heat capacity for a fixed ζ and decreasing $\bar{\alpha}$

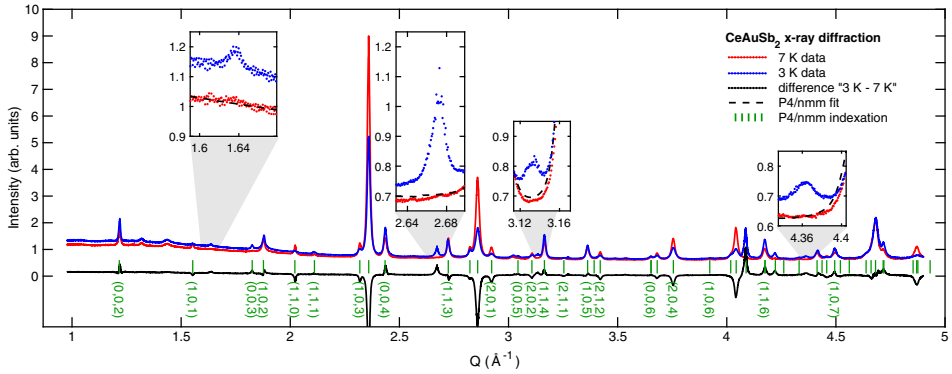

FIG. 2. Synchrotron (20 keV) x-ray powder diffraction patterns of $CeAuSb_2$ obtained above (7 K, red) and below (3 K, blue) the transitions at $T_{N,\mathrm{nem}}$. The difference pattern (black line) emphasizes significant intensity gains, or losses, at most Bragg positions. Green markers and labels indicate the indexation of these peaks in the high-temperature $P4/nmm$ structure. A lattice distortion is not resolved. Below the structural transition, four additional Bragg peaks are observed (see insets), which are not indexed by the parent phase.

towards the critical value $\bar{\alpha}_c$, below which the magnetic transition becomes first order but remains distinct from the nematic transition (see Supplemental Material [45] for details). Figure 1(b) shows the calculated heat capacity C/T as a function of reduced temperature $\tilde{t} \propto (T - T_N)/T_N$. Upon approaching $\bar{\alpha}_c$, the specific heat peak at T_N increases at a faster rate than the jump at T_{nem}, and the separation between the two transition temperatures decreases, signaling the approach of a first-order magnetic transition. In order to compare our model with the experimental results in Fig. 1(a), which do not show sharp jumps, we include weak disorder by considering a distribution of T_N^0 values, yielding a smooth temperature dependence of the derivative of C/T [see inset of Fig. 1(b)]. The comparison shows that $\mathrm{d}(C/T)/\mathrm{d}\tilde{t} = 0$ at T_N and $\mathrm{d}(C/T)/\mathrm{d}\tilde{t}$ has a minimum at T_{nem} and suggests that $CeAuSb_2$ at ambient conditions is close to $\bar{\alpha} = 2.7$. Our model predicts that below $\bar{\alpha}_c$, both nematic and magnetic phase transitions become first order and simultaneous at $T_{\mathrm{nem}} = T_N$. Without a full microscopic theory, it is difficult to determine how the Ginzburg-Landau coefficients depend on the experimentally relevant parameters such as pressure and magnetic field. However, as we show below, our experimental data under applied pressure suggest that hydrostatic pressure might reduce $\bar{\alpha}$, thus making the transition first order and simultaneous.

Now, we turn our attention to the field and pressure dependence of the coupled transitions in $CeAuSb_2$. Figure 3(a) shows the temperature dependence of the in-plane resistivity (ρ_{ab}) of $CeAuSb_2$ under various pressures up to 2.66 GPa. At ambient pressure, a sharp drop in ρ_{ab} occurs at about 6.8 K. As shown in Fig. 3(b), at low pressure, a single peak marked by orange arrows occurs in $\mathrm{d}\rho/\mathrm{d}T$. Within the resolution of these data ($\Delta T \sim 0.08$ K), this single peak likely encloses both T_N and T_{nem} found in C/T, $\mathrm{d}\chi/\mathrm{d}T$, and $\Delta L/L$ ($\Delta T \sim 0.01$, 0.02, and 0.005 K, respectively). With increasing pressure, $T_N + T_{\mathrm{nem}}$ is suppressed to 5 K at 2.24 GPa. Above 2.24 GPa, however, the single peak splits into two peaks in $\mathrm{d}\rho/\mathrm{d}T$, which are indicated by black and red arrows, respectively. Note that T_{N2} marks a shoulderlike broad peak that increases with increasing pressure and $T_{\mathrm{nem}} = T_N$ marks a sharp symmetric peak that decreases up to 2.52 GPa but increases above 2.52 GPa. We discuss the origin of these transitions below. Above 2.16 GPa, the results from increasing- and decreasing-temperature ramps are shown together in Fig. 3(b), which are indicated by solid and open symbols, respectively. Interestingly, a hysteresis appears at $T_{\mathrm{nem}} = T_N$ in $\mathrm{d}\rho/\mathrm{d}T$, pointing to a first-order phase transition. Hysteresis is not typical of a naked antiferromagnetic (AFM) transition but rather suggests the development of a multicomponent state. At T_{N2} and $T_N + T_{\mathrm{nem}}$, however, hysteresis is not observed in the resistivity. To shed light on the temperature-pressure phase diagram shown in Fig. 3(c), we turn to the pressure dependence of the initially coupled transitions estimated via the Ehrenfest relation

$$\frac{dT_{N/\mathrm{nem}}}{dP} = \frac{V_m \Delta\beta}{\Delta C/T}, \tag{2}$$

where V_m is the molar volume, and $\Delta\beta$ and $\Delta C/T$ are changes of the volume thermal expansion coefficient and the specific heat divided by temperature at the transition. By using the experimental values of β and C/T at ambient pressure, we obtain $\mathrm{d}T_N/\mathrm{d}P = 0.37$ K/GPa and $\mathrm{d}T_{\mathrm{nem}}/\mathrm{d}P = -0.77$ K/GPa (see Fig. S3 [45]); i.e., T_{nem} would be suppressed with pressure, whereas T_N would be enhanced with pressure. These transitions, however, are coupled at low pressures, and the sum of the calculated $\mathrm{d}T/\mathrm{d}P$ values (−0.4 K/GPa) is in good agreement with the experimental pressure dependence of the coupled transition, $\mathrm{d}(T_N + T_{\mathrm{nem}})/\mathrm{d}P \approx -0.45$ K/GPa. Similarly, the volume thermal-expansion coefficient of pnictides such as LaFeAsO and $BaFe_2As_2$ shows two peaks with opposite signs caused by the nematic and magnetic transitions, which would naively suggest that the pressure dependence

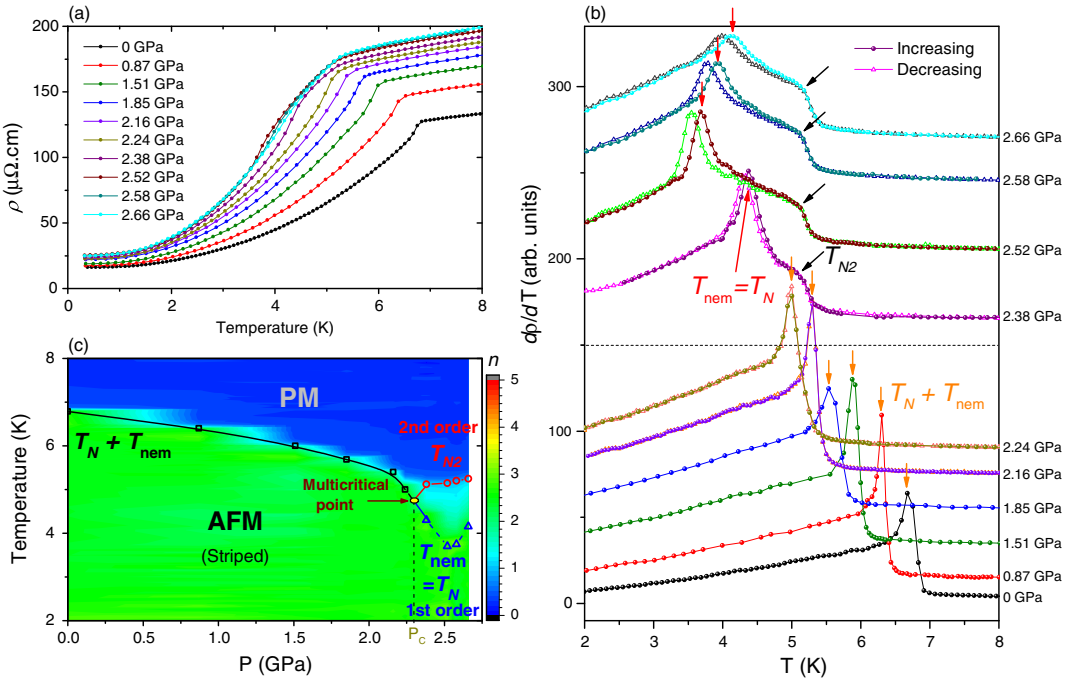

FIG. 3. (a) Temperature dependence of the in-plane electrical resistivity, ρ_{ab}, for $CeAuSb_2$ at pressures to 2.66 GPa. (b) Temperature derivative of ρ_{ab} under pressure. Data at different pressures are shifted for clarity. Arrows indicate peak positions: orange, black, and red arrows for $T_N + T_{\rm nem}$, T_{N2}, and $T_{\rm nem} = T_N$, respectively. Above 2.16 GPa, the results from increasing- and decreasing-temperature ramps are indicated by solid and open symbols, respectively. (c) T-P phase diagram of $CeAuSb_2$ in zero applied field. Colors represent the local exponent, $n = \partial \ln \Delta\rho / \partial \ln T$.

of the two transitions would be opposite [47,48]. These two transitions, however, also decrease together with pressure due to their coupling [49,50]. In our results, the fact that T_{N2} increases with pressure above the critical pressure suggests that it is associated with a different ordered state not coupled to a tetragonal-symmetry breaking, whose origin will be discussed below.

The temperature-pressure false-color map of the local exponent n of the temperature dependence of ρ_{ab} is shown in Fig. 3(c), where $n = \partial \ln \Delta\rho / \partial \ln T$ and $\Delta\rho = \rho_{ab} - \rho_0 = AT^n$. The contour map in Fig. 3(c) provides a proxy for the magnetic scattering in different regions of the phase diagram. Above P_c, the green region ($n \approx 2$) below $T_{\rm nem} = T_N$ displays the same behavior as the zero-pressure phase, indicating that the magnetic phase is striped AFM, whereas below T_{N2} the light-blue region indicates a distinct behavior ($n \approx 1.2$). In Fig. 5, we show that the power-law behavior in the light-blue region at high pressure is similar to the behavior of the multi-q AFM phase at ambient pressure and high fields. Therefore, our results suggest that at P_c, the coupled transition at $T_N + T_{\rm nem}$ becomes (1) a second-order AFM transition to the multi-q phase at T_{N2} and (2) a simultaneous first-order structural and magnetic phase transition to the stripe phase at $T_{\rm nem} = T_N$ due to a finite magnetoelastic coupling. This case suggests the existence of a multicritical point at P_c indicated by a yellow circle in Fig. 3(c) at which four phases meet: a disordered phase PM, a paramagnetic-nematic phase PMnem, an antiferromagnetically ordered stripe-nematic phase AFM(S)nem, and an antiferromagnetically ordered multi-q phase AFM(M).

Evidence for a hysteretic first-order transition is further confirmed in Fig. 4(a), which shows the field dependence of the in-plane resistivity under various pressures, for increasing- and decreasing-field ramps applied along the c axis. At 0.3 K, the first MM transition field H_{c1} and the second MM transition field H_{c2} do not change with increasing pressure as shown in Fig. 4(a). At low pressure, the magnetoresistance between H_{c1} and H_{c2} monotonically increases with increasing field, in agreement with Ref. [19]. Above 2.16 GPa, however, a hysteretic steplike anomaly at H^* is observed between H_{c1} and H_{c2}. Note that H^* decreases with increasing pressure and temperature (see Fig. S4 [45]). Figures 4(b) and 4(c) show the temperature dependence of ρ_{ab} and $\mathrm{d}\rho/\mathrm{d}T$ at representative pressures for $CeAuSb_2$ in an applied magnetic field. At 1.85 GPa, the coupled transition at $T_N + T_{\rm nem}$ turns into two transitions at T^* and T_{N2} above H_{c1}. The new field-induced phase transition at T^* ($H > H_{c1}$) matches the transition at H^* (see Fig. S7 [45]).

Figure 5 displays the temperature-magnetic-field false-color map of the local exponent n of ρ_{ab} for representative pressures, where $n = \partial \ln \Delta\rho / \partial \ln T$ and $\Delta\rho = \rho_{ab} - \rho_0 = AT^n$. The contour maps show the presence of two distinct regions in the AFM phase diagrams. The single-q region (S) displays a local exponent $n \approx 2$, whereas the multi-q

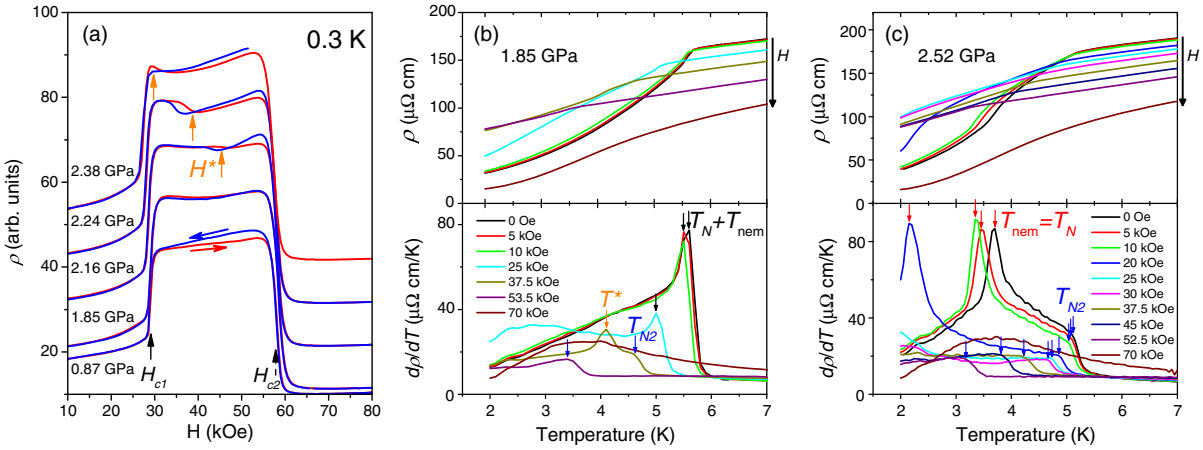

FIG. 4. (a) In-plane electrical resistivity of $CeAuSb_2$ as a function of magnetic field applied along the c axis at 0.3 K for representative pressures. Magnetoresistance from increasing- and decreasing-field ramps is plotted by red and blue lines, respectively. Data at different pressures are shifted for clarity. (b,c) Low-temperature in-plane electrical resistivity for various applied magnetic fields at 1.85 GPa and 2.52 GPa. Here, ρ_{ab} and $d\rho/dT$ as a function of temperature are shown in the upper and bottom panels, respectively.

region (M) reveals $n \approx 1$ at ambient pressure. The similar color map for the exponent n in Ref. [18] does not display the difference of magnetic scattering between distinct magnetic phases because the color scale of that map is not segmented enough to show the difference of n between 1 and 2. At 2.52 GPa, the contour map indicates that the pressure-induced new phase in zero field below T_{N2} is related to the field-driven multi-q phase at ambient pressure. In order to understand the origin of T^* and the other phases denoted by (M', M", and M*) under pressure, the underlying magnetic structures will have to be determined by neutron or nuclear magnetic resonance measurements under applied pressure and field. Interestingly, experiments on $CeAuSb_2$ under uniaxial strain along the [100] direction also suggest additional magnetic phases [30,31]. In particular, the $H-T$ phase diagram under applied compression along the [100] direction resembles our phase diagram in Fig. 5(d), but it is not precisely the same [31]. Different effects caused by uniaxial and hydrostatic applied pressure have also been observed in the Fe-based superconductors [51]. Finally, we note that the tricritical point of H_{c2} indicated by yellow circles in Fig. 5 is not suppressed to zero temperature with pressure (see Ref. [45]).

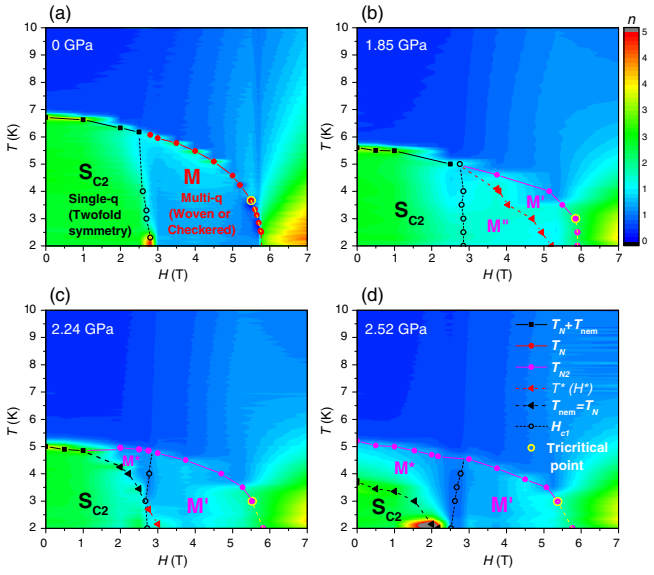

FIG. 5. False-color map of the effective resistivity exponent n in the H-T phase diagram at (a) 0 GPa, (b) 1.85 GPa, (c) 2.24 GPa, and (d) 2.52 GPa. The green region denotes the single-q stripe phase (S_{C2}), and the light-blue region denotes the other possible AFM phases (M, M', M", and M*).

IV. DISCUSSION

Striped magnetic phases are ubiquitous in strongly correlated materials [26,29,52,53], and unconventional superconductivity is arguably intertwined with spin and charge stripe correlations in the copper oxides and iron-based materials [27]. However, superconductivity is absent in, e.g., nickel oxides, which also host a stripe pattern within the NiO_2 planes analogous to the CuO_2 planes in copper oxides [28]. Here, we show that the f-electron system $CeAuSb_2$ also supports a nematic state in the absence of superconductivity. In $CeAuSb_2$, the signatures of two phase transitions in various thermodynamic measurements are very similar to signatures for nematic and magnetic transitions in the Fe-based superconductors. Despite the opposite sign of the calculated dT/dP for the different transitions, the coupled transitions decrease together with pressure initially, as in the iron-pnictide compounds. Unlike the Fe-based materials, however, in $CeAuSb_2$, an additional transition appears at P_c. Above P_c, this new transition temperature increases with increasing pressure, in contrast to the lower-temperature transition.

The key difference between $CeAuSb_2$ and the Fe-based materials is the absence of superconductivity under pressure. Though nematicity may boost Cooper pairing in the iron-based superconductors, nematic fluctuations may be weak in $CeAuSb_2$ due to the first-order nature of the nematic transition and the change in the ground-state wave function of the system at P_c. Previous pressure work revealed that two energy scales, one associated with Kondo coherence and the other with crystalline electric field (CEF) splitting, become similar at P_c. As a result, wave functions of the excited crystal-field levels become admixed into the ground state, hindering formation of a fully Kondo coherent ground state, yet allowing new magnetic orders that lead to a magnetic state that persists to over 4 GPa [20]. Because of the competing magnetic interactions known to be present in the class of localized materials, various magnetic orders compete under pressure and magnetic field. The family member $CeAgSb_2$ also shows a new magnetic phase above $P_c \sim 2.7$ GPa, and $T_{\max}$ exhibits unexpected negative pressure dependence above P_c, which may be due to the influence of a low-lying CEF level $\Delta_1 \sim 50$ K [44,54]. Neutron and x-ray scattering studies would be valuable to shed light not only on the crystal-field wave functions at ambient conditions but also on their evolution under applied pressure and magnetic fields.

V. CONCLUSIONS

In summary, we have constructed the temperature-magnetic-field phase diagrams of $CeAuSb_2$ under applied pressure. Bulk thermodynamic probes reveal two closely lying phase transitions at $T_N = 6.3$ K and $T_{\text{nem}} = 6.5$ K, and x-ray diffraction measurements verify that striped magnetic order is connected to a structural phase transition at ambient pressure. Our theoretical model suggests that stripe magnetic order is preceded by a nematic phase in $CeAuSb_2$. The discovery of a putative nematic phase in an f-electron material at zero magnetic field provides an unexplored framework for nematicity, though superconductivity, if present, remains to be discovered.

ACKNOWLEDGMENTS

Work at Los Alamos was performed under the auspices of the U.S. Department of Energy, Office of Basic Energy Sciences, Division of Materials Science and Engineering. S. S. acknowledges support through the Laboratory Directed Research and Development program. Scanning electron microscope and energy dispersive x-ray measurements were performed at the Center for Integrated Nanotechnologies, an Office of Science User Facility operated for the U.S. Department of Energy Office of Science. Theory work (R. M. F.) was supported by the U.S. Department of Energy Office of Science, Basic Energy Sciences, under Award No. DE-SC0012336 and, during completion of the work, under Award No. DE-SC0020045. X. W. is supported by the University of Chicago Materials Research Science and Engineering Center, which is funded by the National Science Foundation under Grant No. DMR-1420709. R. D. d. R. and D. C. acknowledge financial support from the Brazilian agencies CAPES and FAPESP (Grants No. 2018/00823-0 and No. 2018/22883-5).

[1] G. R. Stewart, *Heavy-Fermion Systems*, Rev. Mod. Phys. **56**, 755 (1984).
[2] Z. Fisk, D. W. Hess, C. J. Pethick, D. Pines, J. L. Smith, J. D. Thompson, and J. O. Willis, *Heavy-Electron Metals: New Highly Correlated States of Matter*, Science **239**, 33 (1988).
[3] P. Coleman, *Heavy Fermions: Electrons at the Edge of Magnetism*, in *Handbook of Magnetism and Advanced Magnetic Materials* (John Wiley & Sons, Chichester, UK, 2007), pp. 95–148.
[4] P. Coleman, *Heavy Fermions: Dimensions Are Critical*, Nat. Mater. **11**, 185 (2012).
[5] H. v. Löhneysen, A. Rosch, M. Vojta, and P. Wölfle, *Fermi-Liquid Instabilities at Magnetic Quantum Phase Transitions*, Rev. Mod. Phys. **79**, 1015 (2007).
[6] G. R. Stewart, *Non-Fermi-Liquid Behavior in d- and f-Electron Metals*, Rev. Mod. Phys. **73**, 797 (2001).
[7] T. Shibauchi, A. Carrington, and Y. Matsuda, *A Quantum Critical Point Lying Beneath the Superconducting Dome in Iron Pnictides*, Annu. Rev. Condens. Matter Phys. **5**, 113 (2014).
[8] E. Fradkin, S. A. Kivelson, M. J. Lawler, J. P. Eisenstein, and A. P. Mackenzie, *Nematic Fermi Fluids in Condensed Matter Physics*, Annu. Rev. Condens. Matter Phys. **1**, 153 (2010).
[9] R. M. Fernandes, A. V. Chubukov, and J. Schmalian, *What Drives Nematic Order in Iron-Based Superconductors?*, Nat. Phys. **10**, 97 (2014).
[10] S. Lederer, Y. Schattner, E. Berg, and S. A. Kivelson, *Superconductivity and Non-Fermi Liquid Behavior Near a Nematic Quantum Critical Point*, Proc. Natl. Acad. Sci. U.S.A. **114**, 4905 (2017).
[11] F. Ronning, T. Helm, K. R. Shirer, M. D. Bachmann, L. Balicas, M. K. Chan, B. J. Ramshaw, R. D. McDonald, F. F. Balakirev, M. Jaime, E. D. Bauer, and P. J. W. Moll, *Electronic In-Plane Symmetry Breaking at Field-Tuned Quantum Criticality in* $CeRhIn_5$, Nature (London) **548**, 313 (2017).
[12] R. Okazaki, T. Shibauchi, H. J. Shi, Y. Haga, T. D. Matsuda, E. Yamamoto, Y. Onuki, H. Ikeda, and Y. Matsuda, *Rotational Symmetry Breaking in the Hidden-Order Phase of* URu_2Si_2, Science **331**, 439 (2011).
[13] P. F. S. Rosa, S. M. Thomas, F. F. Balakirev, E. D. Bauer, R. M. Fernandes, J. D. Thompson, F. Ronning, and M. Jaime, *Enhanced Hybridization Sets the Stage for Electronic Nematicity in* $CeRhIn_5$, Phys. Rev. Lett. **122**, 016402 (2019).
[14] G. G. Lesseux, H. Sakai, T. Hattori, Y. Tokunaga, S. Kambe, P. L. Kuhns, A. P. Reyes, J. D. Thompson, P. G. Pagliuso, and R. R. Urbano, *Orbitally Defined Field-Induced Electronic State in a Kondo Lattice*, arXiv:1905.02861.

[15] Y. Muro, N. Takeda, and M. Ishikawa, *Magnetic and Transport Properties of Dense Kondo Systems,* $CeTSb_2$ *(*T = Ni*, Cu, Pd and Ag)*, J. Alloys Compd. **257**, 23 (1997).

[16] A. Thamizhavel, T. Takeuchi, T. Okubo, M. Yamada, R. Asai, S. Kirita, A. Galatanu, E. Yamamoto, T. Ebihara, Y. Inada, R. Settai, and Y. Onuki, *Anisotropic Electrical and Magnetic Properties of* $CeTSb_2$ *(*T = Cu*, Au, Ni) Single Crystals*, Phys. Rev. B **68**, 054427 (2003).

[17] G. André, F. Bourée, M. Kolenda, B. Leśniewska, A. Oleś, and A. Szytuła, *Magnetic Structures of* $RAgSb_2$ *Compounds*, Physica B (Amsterdam) **292**, 176 (2000).

[18] L. Balicas, S. Nakatsuji, H. Lee, P. Schlottmann, T. P. Murphy, and Z. Fisk, *Magnetic Field-Tuned Quantum Critical Point in* $CeAuSb_2$, Phys. Rev. B **72**, 064422 (2005).

[19] L. Zhao, E. A. Yelland, J. A. N. Bruin, I. Sheikin, P. C. Canfield, V. Fritsch, H. Sakai, A. P. Mackenzie, and C. W. Hicks, *Field-Temperature Phase Diagram and Entropy Landscape of* $CeAuSb_2$, Phys. Rev. B **93**, 195124 (2016).

[20] S. Seo, V. A. Sidorov, H. Lee, D. Jang, Z. Fisk, J. D. Thompson, and T. Park, *Pressure Effects on the Heavy-Fermion Antiferromagnet* $CeAuSb_2$, Phys. Rev. B **85**, 205145 (2012).

[21] H. Flandorfer, O. Sologub, C. Godart, K. Hiebl, A. Leithe-Jasper, P. Rogl, and H. Noël, *On the Cerium Valence in Ternary Compounds* $CeMSb_2$ *and* $CeM'Bi_2$*; M=Mn, Fe, Co, Ni, Cu, Zn, Pd, Ag, Au and M'* = Ni*, Cu, Zn, Ag*, Solid State Commun. **97**, 561 (1996).

[22] G. G. Marcus, D.-J. Kim, J. A. Tutmaher, J. A. Rodriguez-Rivera, J. O. Birk, C. Niedermeyer, H. Lee, Z. Fisk, and C. L. Broholm, *Multi-q Mesoscale Magnetism in* $CeAuSb_2$, Phys. Rev. Lett. **120**, 097201 (2018).

[23] C. Adriano, P. F. S. Rosa, C. B. R. Jesus, J. R. L. Mardegan, T. M. Garitezi, T. Grant, Z. Fisk, D. J. Garcia, A. P. Reyes, P. L. Kuhns, R. R. Urbano, C. Giles, and P. G. Pagliuso, *Physical Properties and Magnetic Structure of the Intermetallic* $CeCuBi_2$ *Compound*, Phys. Rev. B **90**, 235120 (2014).

[24] S. M. Thomas, P. F. S. Rosa, S. B. Lee, S. A. Parameswaran, Z. Fisk, and J. Xia, *Hall Effect Anomaly and Low-Temperature Metamagnetism in the Kondo Compound* $CeAgBi_2$, Phys. Rev. B **93**, 075149 (2016).

[25] J. M. Allred, K. M. Taddei, D. E. Bugaris, M. J. Krogstad, S. H. Lapidus, D. Y. Chung, H. Claus, M. G. Kanatzidis, D. E. Brown, J. Kang, R. M. Fernandes, I. Eremin, S. Rosenkranz, O. Chmaissem, and R. Osborn, *Double-Q Spin-Density Wave in Iron Arsenide Superconductors*, Nat. Phys. **12**, 493 (2016).

[26] S. Mori, C. H. Chen, and S.-W. Cheong, *Pairing of Charge-Ordered Stripes in* $(La, Ca)MnO_3$, Nature (London) **392**, 473 (1998).

[27] J. M. Tranquada, B. J. Sternlieb, J. D. Axe, Y. Nakamura, and S. Uchida, *Evidence for Stripe Correlations of Spins and Holes in Copper Oxide Superconductors*, Nature (London) **375**, 561 (1995).

[28] C. H. Chen, S.-W. Cheong, and A. S. Cooper, *Charge Modulations in* $La_{2-x}Sr_xNiO_{4+y}$*: Ordering of Polarons*, Phys. Rev. Lett. **71**, 2461 (1993).

[29] T. Vogt, P. M. Woodward, P. Karen, B. A. Hunter, P. Henning, and A. R. Moodenbaugh, *Low to High Spin-State Transition Induced by Charge Ordering in Antiferromagnetic* $YBaCo_2O_5$, Phys. Rev. Lett. **84**, 2969 (2000).

[30] J. Park, H. Sakai, O. Erten, A. P. Mackenzie, and C. W. Hicks, *Effect of Applied Orthorhombic Lattice Distortion on the Antiferromagnetic Phase of* $CeAuSb_2$, Phys. Rev. B **97**, 024411 (2018).

[31] J. Park, H. Sakai, A. P. Mackenzie, and C. W. Hicks, *Effect of Uniaxial Stress on the Magnetic Phases of* $CeAuSb_2$, Phys. Rev. B **98**, 024426 (2018).

[32] M. D. Lumsden and A. D. Christianson, *Magnetism in Fe-Based Superconductors*, J. Phys. Condens. Matter **22**, 203203 (2010).

[33] C. W. Chu, F. Chen, M. Gooch, A. M. Guloy, B. Lorenz, B. Lv, K. Sasmal, Z. J. Tang, J. H. Tapp, and Y. Y. Xue, *The Synthesis and Characterization of LiFeAs and NaFeAs*, Physica C **469**, 326 (2009).

[34] C. Xu, M. Müller, and S. Sachdev, *Ising and Spin Orders in the Iron-Based Superconductors*, Phys. Rev. B **78**, 020501(R) (2008).

[35] C. Fang, H. Yao, W.-F. Tsai, J. P. Hu, and S. A. Kivelson, *Theory of Electron Nematic Order in LaFeAsO*, Phys. Rev. B **77**, 224509 (2008).

[36] R. M. Fernandes, A. V. Chubukov, J. Knolle, I. Eremin, and J. Schmalian, *Preemptive Nematic Order, Pseudogap, and Orbital Order in the Iron Pnictides*, Phys. Rev. B **85**, 024534 (2012).

[37] R. M. Fernandes, P. P. Orth, and J. Schmalian, *Intertwined Vestigial Order in Quantum Materials: Nematicity and Beyond*, Annu. Rev. Condens. Matter Phys. **10**, 133 (2019).

[38] K. A. Lorenzer, A. M. Strydom, A. Thamizhavel, and S. Paschen, *Temperature-Field Phase Diagram of Quantum Critical* $CeAuSb_2$, Phys. Status Solidi B **250**, 464 (2013).

[39] A. Eiling and J. S. Schilling, *Pressure and Temperature Dependence of Electrical Resistivity of Pb and Sn from 1-300K and 0–10 GPa–Use as Continuous Resistive Pressure Monitor Accurate over Wide Temperature Range; Superconductivity under Pressure in Pb, Sn and In*, J. Phys. F **11**, 623 (1981).

[40] F. A. Lima, M. E. Saleta, R. J. S. Pagliuca, M. A. Eleotério, R. D. Reis, J. Fonseca Júnior, B. Meyer, E. M. Bittar, N. M. Souza-Neto, and E. Granado, *XDS: A Flexible Beamline for X-Ray Diffraction and Spectroscopy at the Brazilian Synchrotron*, J. Synchrotron Radiat. **23**, 1538 (2016).

[41] C. R. Rotundu and R. J. Birgeneau, *First- and Second-Order Magnetic and Structural Transitions in* $BaFe_{2(1-x)}Co_{2x}As_2$, Phys. Rev. B **84**, 092501 (2011).

[42] E. Gati, L. Xiang, S. L. Bud'ko, and P. C. Canfield, *Role of the Fermi Surface for the Pressure-Tuned Nematic Transition in the* $BaFe_2As_2$ *Family*, Phys. Rev. B **100**, 064512 (2019).

[43] T. Takeuchi, T. Inoue, K. Sugiyama, D. Aoki, Y. Tokiwa, Y. Haga, K. Kindo, and Y. Onuki, *Magnetic and Thermal Properties of* $CeIrIn_5$ *and* $CeRhIn_5$, J. Phys. Soc. Jpn. **70**, 877 (2001).

[44] T. Takeuchi, A. Thamizhavel, T. Okubo, M. Yamada, N. Nakamura, T. Yamamoto, Y. Inada, K. Sugiyama, A. Galatanu, E. Yamamoto, K. Kindo, T. Ebihara, and Y. Onuki, *Anisotropic, Thermal, and Magnetic Properties of* $CeAgSb_2$*: Explanation via a Crystalline Electric Field Scheme*, Phys. Rev. B **67**, 064403 (2003).

[45] See Supplemental Material at http://link.aps.org/supplemental/10.1103/PhysRevX.10.011035 for a detailed discussion of the theoretical model and experimental results.

[46] O. Sologub, K. Hiebl, P. Rogl, H. Noël, and O. Bodak, *On the Crystal Structure and Magnetic Properties of the Ternary Rare Earth Compounds* $RETSb_2$ *with* RE = Rare *Earth and* T = Ni*, Pd, Cu and Au*, J. Alloys Compd. **210**, 153 (1994).

[47] L. Wang, U. Köhler, N. Leps, A. Kondrat, M. Nale, A. Gasparini, A. de Visser, G. Behr, C. Hess, R. Klingeler, and B. Büchner, *Thermal Expansion of* $LaFeAsO_{1-x}F_x$*: Evidence for High-Temperature Fluctuations*, Phys. Rev. B **80**, 094512 (2009).

[48] S. L. Bud'ko, N. Ni, S. Nandi, G. M. Schmiedeshoff, and P. C. Canfield, *Thermal Expansion and Anisotropic Pressure Derivatives of* T_c *in* $Ba(Fe_{1-x}Co_x)_2As_2$ *Single Crystals*, Phys. Rev. B **79**, 054525 (2009).

[49] H. Okada, K. Igawa, H. Takahashi, Y. Kamihara, M. Hirano, H. Hosono, K. Matsubayashi, and Y. Uwatoko, *Superconductivity under High Pressure in LaFeAsO*, J. Phys. Soc. Jpn. **77**, 113712 (2008).

[50] J. J. Wu, J. F. Lin, X. C. Wang, Q. Q. Liu, J. L. Zhu, Y. M. Xiao, P. Chow, and C. Jin, *Pressure-Decoupled Magnetic and Structural Transitions of the Parent Compound of Iron-Based 122 Superconductors* $BaFe_2As_2$, Proc. Natl. Acad. Sci. (USA) **110**, 17263 (2013).

[51] T. Yamazaki, N. Takeshita, R. Kobayashi, H. Fukazawa, Y. Kohori, K. Kihou, C. H. Lee, H. Kito, A. Iyo, and H. Eisaki, *Appearance of Pressure-Induced Superconductivity in* $BaFe_2As_2$ *under Hydrostatic Conditions and Its Extremely High Sensitivity to Uniaxial Stress*, Phys. Rev. B **81**, 224511 (2010).

[52] D. D. Khalyavin, D. N. Argyriou, U. Amann, A. A. Yaremchenko, and V. V. Kharton, *Low-Temperature Behavior of* $YBaCo_2O_{5.5}$*: Coexistence of Two Spin-State Ordered Phases*, Phys. Rev. B **77**, 064419 (2008).

[53] K. Knizek, Z. Jirak, E. Pollert, F. Zounova, and S. Vratislav, *Structure and Magnetic Properties of* $Pr_{1-x}Sr_xMnO_3$ *Perovskites*, J. Solid State Chem. **100**, 292 (1992).

[54] V. A. Sidorov, E. D. Bauer, N. A. Frederick, J. R. Jeffries, S. Nakatsuji, N. O. Moreno, J. D. Thompson, M. B. Maple, and Z. Fisk, *Magnetic Phase Diagram of the Ferromagnetic Kondo-Lattice Compound* $CeAgSb_2$ *up to 80 kbar*, Phys. Rev. B **67**, 224419 (2003).

Correction: Support information for the 11th author was missing from the Acknowledgments and has been inserted.